Polymer Testing 64 (2017) 83–91

Contents lists available at ScienceDirect

Polymer Testing

journal homepage: www.elsevier.com/locate/polytest

Material Properties

The effect of halloysite nanotubes and N,N′-ethylenebis (stearamide) on morphology and properties of polylactide nanocomposites with crystalline matrix

Miroslaw Pluta [a, *], Joanna Bojda [a], Ewa Piorkowska [a], Marius Murariu [b], Leila Bonnaud [b], Philippe Dubois [b]

[a] Centre of Molecular and Macromolecular Studies, Polish Academy of Sciences, Sienkiewicza 112, 90-363 Lodz, Poland
[b] Center of Innovation and Research in Materials & Polymers (CIRMAP), Laboratory of Polymeric and Composite Materials (LPCM), University of Mons, (UMONS) & Materia Nova Materials R&D Center, Place du Parc 20, 7000 Mons, Belgium

ARTICLE INFO

Article history:
Received 31 July 2017
Accepted 9 September 2017
Available online 14 September 2017

Keywords:
Polylactide
Halloysite nanotubes
Nanocomposites
Mechanical properties
Thermal properties
Optical properties

ABSTRACT

Poly(lactide)/halloysite nanotubes (PLA/HNT) nanocomposites with crystalline matrix were obtained by cold crystallization and examined. Neat HNT and HNT treated with N,N′- ethylenebis(stearamide) (EBS) were used as nanofillers. Reference materials, PLA and PLA/EBS blend, prepared in the same way, were also considered. The influence of HNT and/or EBS content on the crystallinity and morphology of PLA matrix, as well as on the dynamic mechanical and optical properties of the materials, was determined.

The nanocomposites contained well-distributed HNT, with only occasional agglomerates. HNT, EBS-treated HNT and EBS influenced the morphology of the crystalline PLA matrix and the amounts of the disorder α' (termed also δ) and order α crystallographic forms of PLA. Crystallinity increased stiffness of the materials compared to their counterparts with the amorphous matrix. Owing to the crystallinity and the presence of the nanofillers, the storage modulus at 20 °C and 60 °C increased by up to 30 and 60%, respectively, compared to neat amorphous PLA. Interestingly, at lower nanofiller content the crystalline nanocomposites with EBS were more transparent than neat crystalline PLA.

1. Introduction

Polylactide (PLA), a biobased and biodegradable polyester [1], has recently gained enormous attention because of the increasing concern for the environment. PLA is an alternative to some conventional petroleum-based polymers because of its good mechanical performance and processability, together with biocompatiblility, biodegradablity, as well as compostability and recyclability [2–4]. However, there is still great interest in the physical modification of PLA in order to broaden its applications. To improve the toughness and ductility, PLA has been modified e.g. via route termed "rubber toughening" [5], or by plasticization [6,7]. To enhance thermal stability, mechanical, barrier and other properties, PLA has been also filled with organo-modified layered silicates [8,9], carbon nanotubes (CNT) and graphene derivatives [10,11], calcium carbonate [12], powders of zinc oxide, silver, silica, etc. [13–15].

Recently, halloysite nanotubes (HNT) have drawn attention as a new nanofiller for polymers, including PLA. This is because of their advantages of attractive mechanical properties, capability of dispersion in various polymers due to rod-like geometry with high aspect ratio and relatively weak interparticle interactions [16], availability from natural resources and a price less than that of CNT. Filling with HNT can improve the properties of PLA, including mechanical ones, thermal stability, barrier to water vapor, and also nucleation of crystallization [17–19]. To improve the impact strength and/or elongation at break of PLA/HNT nanocomposites, different interfacial modifiers acting as compatibilizers and/or toughening additives have to be used [17,18,20–23], including N,N′-ethylenebis(stearamide) (EBS) [24,25].

EBS is a fatty amide (a synthetic wax) with various applications, e.g. as a dispersing agent or lubricant to enhance processability, to diminish friction and abrasion. It was reported elsewhere that EBS could remain at the PLA/HNT interface; HNT or other nanofillers can be considered as "nano-support" with highly developed surface for EBS, and only excessive EBS fraction can be finely dispersed

* Corresponding author.
E-mail address: mpluta@cbmm.lodz.pl (M. Pluta).

https://doi.org/10.1016/j.polymertesting.2017.09.013
0142-9418/

within the PLA matrix [25]. Amide groups (—CONH—) from EBS can interact with hydroxyl groups from the HNT surface, contributing to better dispersion of the nanofiller. EBS is also known as an effective nucleating agent for PLA [26,27].

In our previous work, amorphous PLA-based nanocomposites with HNT and EBS-treated HNT were examined [28]. The nanocomposites contained well-distributed nanotubes and occasional micron-sized agglomerates, especially at high loading. HNT, EBS-treated HNT and EBS influenced the cold crystallization of PLA. The nanocomposites exhibited increased stiffness and decreased transparency compared to neat PLA.

Generally, commercial PLAs are copolymers of L-lactide and a small amount of D-lactide. The ability of PLA to crystallize is strongly influenced by its enantiomeric composition, and diminishes with increasing content of repeating units of different chirality [29]. PLAs can be quenched to the glassy state and, subsequently, cold-crystallized during heating. The cold crystallization method leads to a more intense spherulite nucleation resulting in finer spherulites and a shorter crystallization time [30]. It is worth noting that shearing of PLA melt can induce the post-shearing crystallization [31]. Crystallinity diminishes the ability of PLA to deform plastically, and slows down biodegradation, but enhances the barrier properties, broadens the temperature range of potential applications and stabilizes shapes of products during processing.

In this work, nanocomposites with crystalline PLA matrix containing either neat HNT or EBS-treated HNT were prepared and examined. The nanofillers strongly affected the morphology of the crystalline matrix. Owing to the crystallinity and the presence of the nanofillers, the storage modulus at 20 °C and 60 °C increased by up to 30 and 60%, respectively, compared to neat amorphous PLA. Interestingly, at lower nanofiller content the crystalline nanocomposites were more transparent than neat crystalline PLA.

2. Experimental

2.1. Materials

Polylactide (PLA) used in the study was commercially available 4032D grade from NatureWorks LLC (Minnetonka, MN). Its weight average molar mass M_w of 130 kg mol^{-1} and dispersity $M_wM_n^{-1}$ of 1.3 were determined by size-exclusion chromatography (SEC) with a multi-angle laser light scattering (MALLS) detector in methylene chloride. According to the supplier, D-lactide and residual monomer contents were 1.4% and 0.14%, respectively, whereas the relative viscosity was 3.94.

The study utilized halloysite ($Al_2Si_2O_5(OH)_4 \times 2\ H_2O$) nanotubes (HNT) as a nanofiller, which were supplied by Aldrich (USA) in powder form. According to the supplier, the diameter of nanotubes was in the range of 30—70 nm, length ranged from 1 to 3 μm, whereas surface area, pore volume, refractive index and density were 64 m^2 g^{-1}, 1.26—1.34 cm^3 g^{-1}, 1.54 and 2.53 g cm^{-3}, respectively. HNT are classified as a 2D nanofiller.

N,N′- ethylenebis(stearamide) (EBS), linear formula $[CH_3(CH_2)_{16}CONHCH_2]_2$, having molar mass of 593.02 g mol^{-1}, melting temperature of 141—146 °C, density of 0.97 g cm^{-3}, was supplied by Sigma—Aldrich (USA). HNT can be effectively coated with EBS to achieve the desired surface properties and dispersion in PLA matrix [25].

2.2. Preparation of nanocomposites and samples

After drying at 100 °C for 48 h, HNT were dry-mixed with EBS, in a laboratory Rondol turbo-mixer, in weight ratios 90:10 and 80:20. Then, the "wet-coating" was carried out in an internal mixer, first for 5 min at 30 rpm, and then for 15 min at 100 rpm. Prior to blending, all the components, that is PLA, HNT and EBS-treated HNT, were dried overnight at 60 °C. After drying, the components were first dry-mixed, and then melt-compounded in a twin-screw co-rotating extruder. Neat PLA and PLA blend with 1.5 wt% of EBS, as reference materials, were processed in the extruder at the same conditions. The nanocomposite preparation was described in detail by us previously [28].

For further studies, films were prepared by compression molding for 3 min in a hydraulic press at 190 °C followed by rapid quenching between aluminum blocks, held at 0 °C. These quenched films, with an amorphous matrix, were studied by us previously [28]. To obtain films with crystalline PLA matrix, the quenched films were cold-crystallized by heating between metal blocks from room temperature (RT) at a rate of about 8—10 °C min^{-1} up to T_a of 120 °C, then holding at T_a for 20 min, and subsequently cooling to RT. This protocol was based on analysis of cold crystallization and melting behavior of the quenched films [28] and previous works [7,32].

The thickness of films for polarized light microscopy (PLM) and for small angle light scattering (SALS) was approx. 0.02 mm and 0.03 mm, respectively. The thickness of films for differential scanning calorimetry (DSC) and light spectroscopy was 0.3 mm. 1 mm thick films were prepared for dynamic mechanical thermal analysis (DMTA), wide angle X-ray diffraction (WAXD) and scanning electron microscopy (SEM).

The PLA/HNT nanocomposites are referred through this paper as, for instance, P3H, where the number stands for the HNT weight content. PLA/(EBS-treated HNT) nanocomposites are referred as, for instance, P3H/C10, where the first number stands for the HNT weight content, whereas the second term represents the weight percentage of EBS relative to HNT; in this case, C10 denotes HNT/EBS weight ratio of 90:10. For clarity, the compositions of all the materials studied are detailed in Table 1. The letters "q" and "c", when used, denote the quenched and crystallized films, respectively.

2.3. Characterization

Thermal behavior of the samples was analyzed by DSC during heating at 10 °C min^{-1} from RT to 190 °C, under a flow of nitrogen using a DSC 2920 (TA Instruments, New Castle, DE).

To characterize the phase structure and morphology of the films by PLM a Nikon Eclipse 80i equipped with a Nikon DS-Fi1 video camera, was used.

The structure of films was also analyzed by a SALS technique using a He-Ne laser, with wavelength (λ) of 632.8 nm, for generating the Hv scattering patterns.

To have an insight into their internal structure, the films were cryo-fractured. In addition, selected materials were microtomed, and the revealed surfaces were enzymatically etched according to a modified method of He et al. [33], described in detail previously [28]. Determination of suitable time of etching, up to 15 min, was

Table 1
Codes and composition of the materials.

Sample code	PLA content (wt %)	HNT content (wt %)	EBS content (wt %)	Weight ratio HNT/EBS
PLA	100	–	–	–
P3H	97	3	–	–
P3H/C10	96.67	3	0.33	90/10
P3H/C20	96.25	3	0.75	80/20
P6H	94	6	–	–
P6H/C10	93.34	6	0.66	90/10
P6H/C20	92.5	6	1.50	80/20
P1.5C	98.5	–	1.50	–

based on preliminary experiments. Then, the surfaces were sputtered with gold using a Jeol Fine Coater 1200 (Tokyo, Japan) and analyzed with SEM Jeol 5500LV operating in the high vacuum mode and at an accelerating voltage of 10 kV.

The films were characterized by WAXD in the reflection mode in 2θ range from 6 to 45° with steps of 0.05°. A wide-angle goniometer, coupled to a sealed tube X-ray generator Philips PW3830 (Eindhoven, The Netherlands) operating at 30 kV and 50 mA, was used. The X-ray beam consisted of the CuK$_\alpha$ radiation (0.154 nm) filtered by a Ni filter and electronically.

DMTA was conducted on rectangular specimens, 17 mm × 10 mm, 1 mm thick, in single cantilever bending mode. A DMTA TA Q-800 Thermal Analyser (TA Instruments) was used, at a frequency of 1 Hz and a heating rate of 2 °C min^{-1} from −10 to 140 °C, under a fixed deformation of 0.5%.

Direct light transmittance (DLT) was measured using a UV-VIS spectrometer, SPECORD S600 diode array instrument (Analytik Jena, Germany), at RT in a range from 200 to 1000 nm, with a resolution of 0.5 nm and using air as a reference. Data were averaged for 5 runs for each 0.3 mm thick film.

3. Results and discussion

3.1. Thermal properties

Fig. 1 shows first heating thermograms of the c-materials, and also cold crystallization exotherms recorded for the starting PLA-based q-materials during heating from RT to T$_a$ at the same rate of 10 °C min^{-1}, from Ref. [28]. The thermogram of cEBS evidences several transitions: four melting endotherms with peaks at about 60, 74, 106 and 146 °C, and one crystallization exotherm with a peak at approx. 80 °C; the corresponding calorimetric parameters are listed in Table 2.

DSC thermogram of the cEBS and its calorimetric parameters are quite similar to those of qEBS [28]. This indicates that qEBS had already crystallized during quenching, whereas heating from RT to T$_a$, followed by 20 min annealing at T$_a$, to produce cEBS, did not induce any marked change in its structure and thermal properties, which are influenced by recrystallization phenomena occurring in this polymer [28,34].

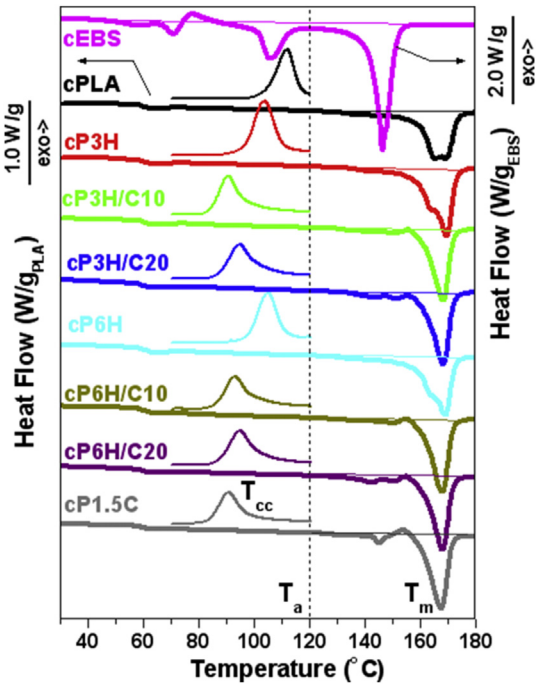

Fig. 1. DSC heating thermograms of c-materials (vertically shifted for clarity). The exotherms from Ref. [28], illustrate cold crystallization behavior of the starting q-materials up to T$_a$.

Table 2
Calorimetric parameters of cEBS. T$_{m1}$, T$_{m2}$, T$_{m3}$, T$_{m4}$ and ΔH$_{m1}$, ΔH$_{m2}$, ΔH$_{m3}$, ΔH$_{m4}$ are the melting peak temperatures and corresponding melting enthalpies, respectively, T$_{cc}$ and ΔH$_{cc}$ denote the cold crystallization peak temperature and enthalpy, respectively.

T$_{m1}$ (°C)	ΔH$_{m1}$ (J/g)	T$_{m2}$ (°C)	ΔH$_{m2}$ (J/g)	T$_{cc}$ (°C)	ΔH$_{cc}$ (J/g)	T$_{m3}$ (°C)	ΔH$_{m3}$ (J/g)	T$_{m4}$ (°C)	ΔH$_{m4}$ (J/g)
59.4	8.8	74.5	9.0	78.0	7.6	106.1	52.1	146.6	129.3

Table 3
Calorimetric parameters of cPLA-based materials. T$_g$ denotes the glass transition temperature, T$_m$ and ΔH$_m$ are the melting peak temperature and melting enthalpy of PLA matrix, the latter calculated by proper subtraction of ΔH$_{m4}$ of EBS fraction. T$_{cc}$ and ΔH$_{cc}$ are the cold crystallization peak temperature [28] and cold crystallization enthalpy of the PLA matrix of starting q-materials during heating, the latter calculated by integration up to T$_a$. X$_c$ and X$_q$ denote corresponding values of mass crystallinity of PLA in the c-materials after annealing at T$_a$ and developed during heating up to T$_a$ at 10 °C min^{-1}, respectively.

Sample code	T$_g$ (°C)	T$_m$ (°C)	ΔH$_m$ (J/g$_{PLA}$)	X$_c$ (wt%)	T$_{cc}$ (°C)	ΔH$_{cc}$ (J/g$_{PLA}$)	X$_q$ /X$_c$
cPLA	61.7	164.9 168.9	42.4	40.0	111.7	30.3	0.71
cP3H	60.8	169.2	47.2	44.5	103.6	38.9	0.82
cP3H/C10	60.5	168.0	40.2	37.9	90.6	32.4	0.81
cP3H/C20	60.1	168.1	43.3	40.8	94.6	31.3	0.73
cP6H	61.8	168.9	44.5	42.0	104.9	34.0	0.76
cP6H/C10	60.4	167.7	40.6	38.3	93.1	29.8	0.73
cP6H/C20	60.5	167.8	41.0	38.7	94.8	30.8	0.75
cP1.5C	59.2	167.2	37.2	35.1	90.7	25.6	0.69

The heating thermograms of cPLA-based materials in Fig. 1 do not show any evidence of cold crystallization. The calorimetric parameters of c-materials are detailed in Table 3. Glass transtion temperatures (T$_g$) of the c-nanocomposites and cPLA were similar, from 60.1 to 61.8 °C, although higher by about 2–4 °C than those of their q-counterparts [28]. The increase of T$_g$ of PLA due to crystallinity was observed by others, especially after annealing [35]. Only cP1.5C exhibited T$_g$ of 59.2 °C, possibly due to lower crystallinity. One can also suspect that the endothermic effects in EBS in the temperature range of glass transition of PLA can slightly affect the determined values of T$_g$ for the EBS-containing materials.

The melting endotherms of the cPLA-based materials started to build up above 120 °C. cPLA exhibited double peak melting behavior, with peak temperatures (T$_m$) at 165 and 169 °C and a low temperature shoulder near 143 °C. The thermograms of cP3H and cP6H were featured by single peaks with T$_m$ at 169 °C with low temperature shoulders at 164–165 °C and close to 143 °C. Such behavior can reflect melting and recrystallization of less stable PLA crystals, the latter contributing further to the melting peak at higher temperature.

The melting process of EBS-containing nanocomposites was more complex, in each case with a small melting endotherm in the range 120–155 °C followed by a main melting peak with T$_m$ at about 168 °C. The small endotherms most probably originated from superposition of melting of EBS and also melting and recrystallization of PLA crystals, possibly connected with the disorder α' - to order α form transition [e.g. 36-38]. This is clearly visible on the thermogram of cP1.5C blend, where a small sharp melting peak of EBS showed up at 145 °C, superimposed on a broad low temperature endotherm of PLA, followed by a small exothermic peak at 154 °C, which is obviously connected with the α′ to α transition

[36–39]. The melting enthalpy (ΔH_m) of neat cPLA and PLA matrix in the c-nanocomposites was 40–47 J g_{PLA}^{-1}, which corresponds to crystallinity of 38–44%, if the heat of fusion of fully crystalline PLA of 106 Jg^{-1} is assumed [40]. cP1.5C exhibited slightly lower X_c of 35%.

Fig. 1 shows that cold crystallization in the materials was greatly advanced during heating to T_a. Moreover, the cold crystallization was influenced by the sample composition [28]. Integration up to T_a of cold crystallization exotherms recorded at 10 °C min^{-1}, permitted to estimate that 70–80% of crystallinity developed during heating and the rest during annealing at T_a.

3.2. Structure

3.2.1. PLM

Fig. 2 compares PLM micrographs of all cPLA-based materials recorded with crossed polarizers. cPLA, cP3H and cP6H revealed fine grain structure. In cP1.5C, fine grains can be also discerned, although with difficulty. However, in the EBS-containing c-nanocomposites only bright spots ascribed to micron-size agglomerates of HNT [28] are clearly visible. Brightening evidences the birefringence resulting from the presence of crystals, although grains are not discernible, most probably because of too small sizes. Similar micrographs were obtained for the c-nanocomposites with higher EBS content (not shown). Fig. 1 and Table 3 indicate lower T_{cc}s of these materials compared to the EBS-free materials, which confirms more intense nucleation in the former, usually also reflected in smaller grain sizes. It is worth noting that EBS is known to nucleate crystallization of PLA [26–28].

3.2.2. SALS

Fig. 3 shows SALS patterns for cPLA and cP6H. Only for the cPLA and c-nanocomposites without EBS were the four-leaf-clover Hv patterns, characteristic of spherulitic structure, obtained. It follows that dispersed HNT did not prevent formation of PLA spherulites. However, for the materials with EBS, the four-leaf-clover patterns were not obtained because of changes in morphology induced by EBS. The average radii of spherulites in the cPLA and cP6H were calculated based on the four-leaf clover SALS patterns according to the following formula [41]:

$$R_{av} = 4.09\lambda/[4\pi \sin(\theta_{max}/2)] \quad (1)$$

where θ_{max} is the angle of the maximum intensity of scattered light in the azimuthal direction of 45°. R_{av} calculated for cPLA and cP6H materials exhibited R_{av} of 2.2 and 1.6 μm, respectively. The decrease of R_{av} for the latter was caused by nucleation activity of HNT, reflected also in the decrease of T_{cc} of this nanocomposite compared to the neat polymer. It is worth noting that the SALS determined R_{av} is a fifth-order average for three-dimensional spherulites [42] and,

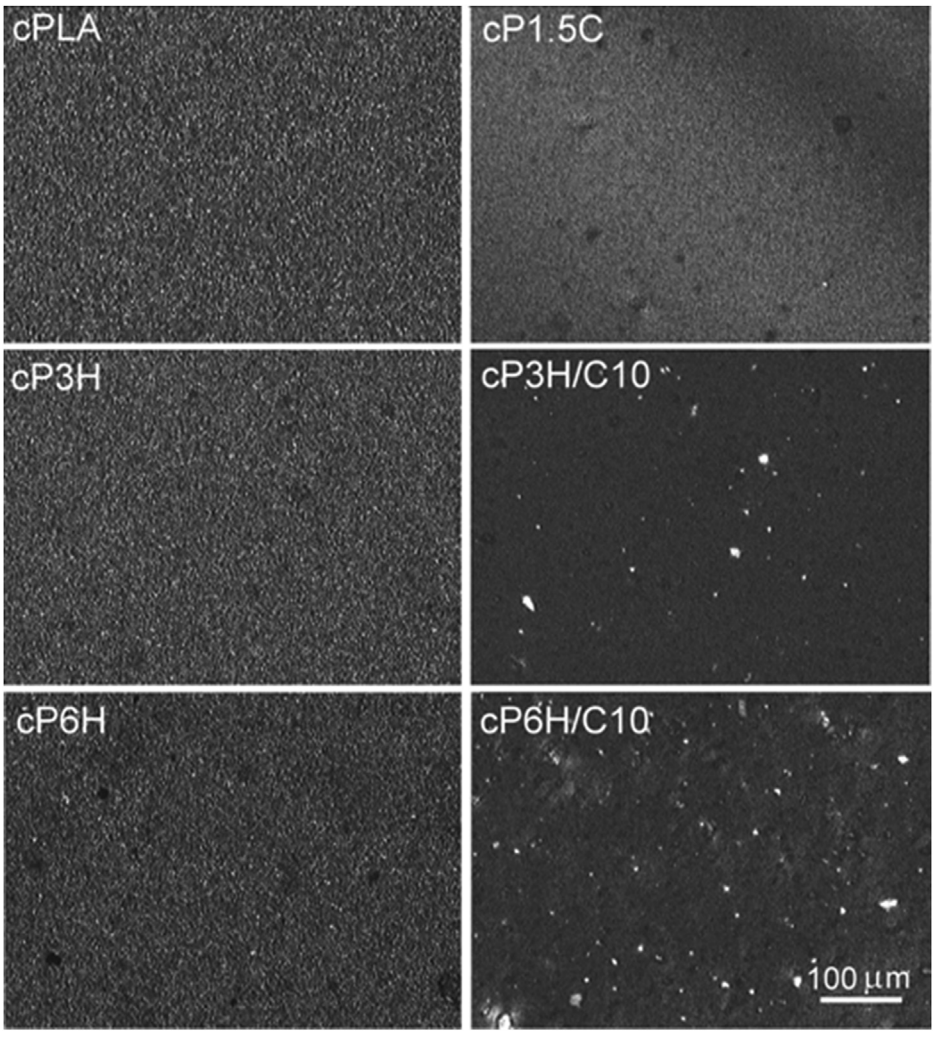

Fig. 2. PLM micrographs of thin films of selected c-materials recorded at RT with crossed polarizers.

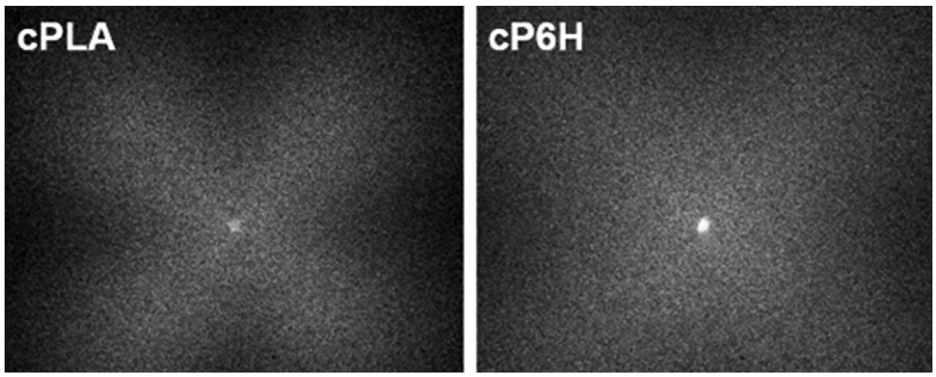

Fig. 3. H_V SALS patterns for cPLA and cP6H.

because of that, is heavily weighted in favor of larger spherulites.

3.2.3. SEM

Fig. 4 shows SEM micrographs of cryo-fractured surfaces of cPLA and cPLA-based materials. The surfaces of c-materials are more developed than their q-counterparts [28] because of the presence of crystalline phase. In cPLA1.5C, submicron inclusions of EBS are clearly visible, as in qcP1.5C [28], evidencing phase separation. In the c-nanocomposites, the EBS inclusions were not observed because the modifier was predominantly located at HNT surfaces [25,28].

SEM micrographs of microtomed and Proteinase K etched surfaces of the selected materials are shown in Fig. 5. Proteinase K is known to degrade L-lactide units, preferentially in the amorphous

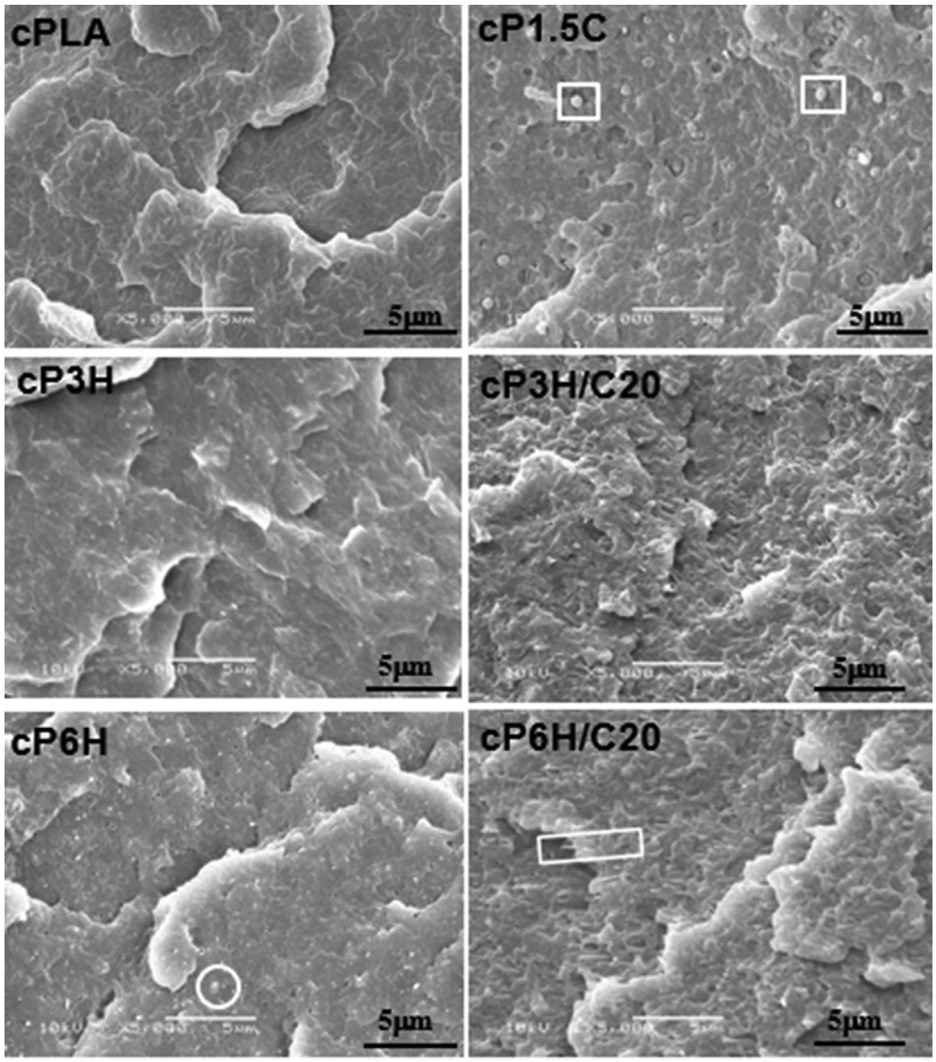

Fig. 4. SEM micrographs of cryo-fractured surfaces of selected c-materials. Markers indicate: squares – EBS inclusions, rectangles – elongated HNT, circles – HNT agglomerates.

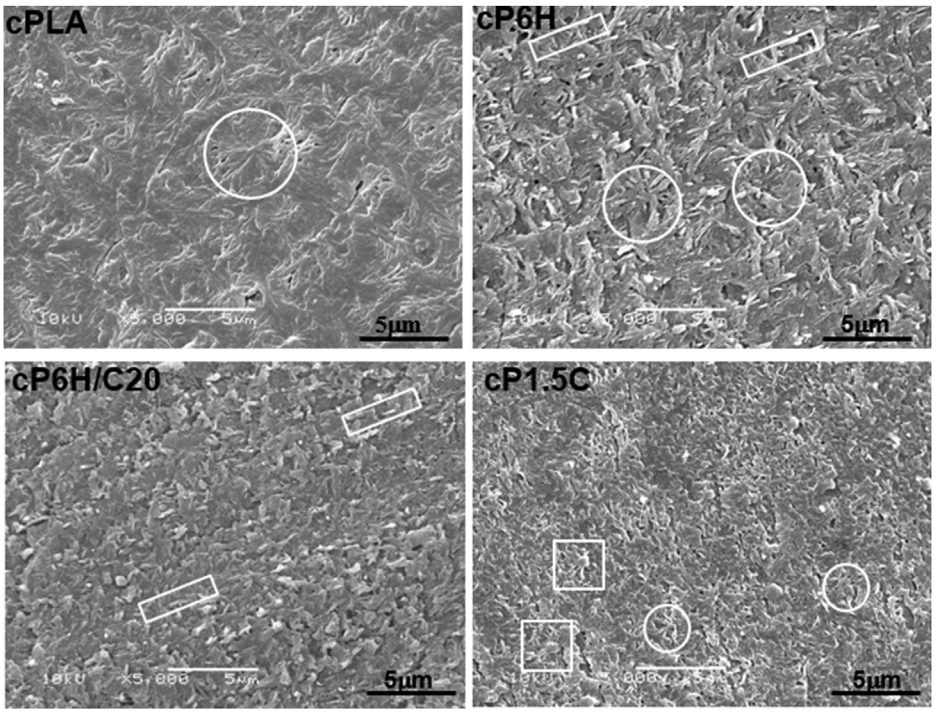

Fig. 5. SEM micrographs of etched microtomed surfaces of selected c-samples. Markers indicate: circles - spherulites, squares – EBS inclusions, rectangles – elongated HNT inclusions.

phase. Spherulites are clearly seen on the surface of the neat cPLA. On the cP6H surface, spherulites are more difficult to distinguish although bunches of lamellae radiating from common centers can be discerned. Roughly determined radii are up to 3 and 2.5 μm for cPLA and cP6H, respectively, which corroborates the SALS results. In EBS-containing materials, polycrystalline aggregates were even more difficult to discern, although in few places small ones with submicron radii could be found. All EBS-containing materials exhibited T_{cc}s lower than those without the modifier, because of nucleating activity of EBS, which obviously decreased the size of polycrystalline aggregates so strongly that they were not clearly detectable in our experiments. The micrographs also reveal tubular particles and agglomerates of HNT in the nanocomposites, whereas bunches of lamellae emanating from surfaces of submicron EBS inclusions in cP1.5C confirm the strong ability of EBS to nucleate crystallization of PLA.

3.2.4. WAXD

Fig. 6 shows X-ray diffractograms of selected c-materials. For all the materials, cPLA and c-nanocomposites, diffraction peaks characteristic of crystalline PLA are observed. Indexing of the reflections follows that in Ref. [39]. In addition, the diffractograms of c-nanocomposites exhibit weak reflections typical of HNT [28]. Interestingly, the (110)/(200) and (203) reflections of c-nanocomposites are shifted to lower 2θ angles compared to neat cPLA. This indicates the presence of the disorder α′ form, which is consistent with the crystallization conditions of the materials studied. The α′ form was found by Zhang et al. [37] in poly(L-lactide) (PLLA) crystallized isothermally below 120 °C. It is worth noting that others [38] reported the presence of the α′ form in PLLA cold-crystallized isothermally at temperatures up to 125 °C. On the other hand, (210) and (103) reflections on the diffractograms confirm the presence of the order α form, although (103) reflection overlapps with a reflection from HNT at 2θ close to 12°. T_{cc}s of EBS-free materials were higher than those of EBS-containing materials, hence the latter should contain larger α′ fractions. The heating thermogram of cPLA1.5C in Fig. 1 exhibits a small exothermic peak at 154 °C, typical of the α′ to α transition. Indeed, in cP1.5C, after heating to 156 °C and cooling at 30 °C min^{-1} to RT, the (110)/(200) and (201) reflections are shifted to larger 2θ angles, as shown in the inset of Fig. 6.

It is worth adding that the polymorphic structure markedly influences the mechanical properties of PLLA; the α modification results in a higher Young's modulus, however, in a lower elongation at break compared to the α′ form [43]. We note that the α′ form was more recently analysed by Wasanasuk and Tashiro [44] and termed as the δ form.

3.3. Viscoelastic properties

Fig. 7 demonstrates the temperature dependencies of the storage (E′) and loss (E″) moduli of selected materials. The T_g taken as E″ peak temperature (T_g(E″)), the relative mechanical loss magnitude (MLM) connected with the glass transition as well as the values of E′ determined at 20, 60 and 80 °C are collected in Table 4. MLM was calculated for each c-material as the ratio of area under E″ peak, integrated from 30 to 110 °C, to that of neat cPLA.

It follows that the T_g(E″) values of cPLA and c-nanocomposites are similar, 70–71 °C, and are not affected by the composition. Only cP1.5C exhibits lower T_g(E″) of approx. 68 °C, most probably due to smaller crystallinity, as already found by DSC. Crystallinity broadened the glass transition and also increased T_g(E″) compared to approx. 63 °C measured for the q-materials previously [28]. The relative mechanical loss magnitude (MLM) increased with HNT content and also was enlarged by the presence of EBS, to 1.33 for cP6H/C20, because of contribution of energy dissipation at the nanofiller/PLA matrix interface [45]. Crystals introduce structural heterogeneity which also contributes to the increase of the area under E″ peak, as can be seen from comparison of cPLA and qPLA [28].

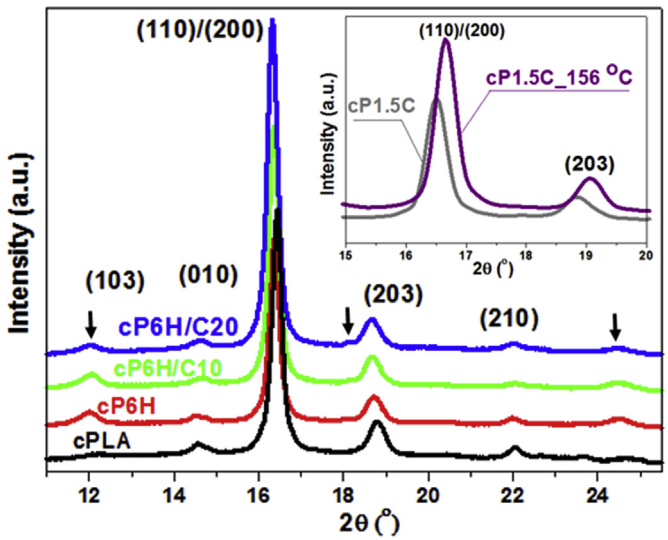

Fig. 6. X-ray diffractograms of neat cPLA and c-nanocomposites with 6 wt% of HNT. Arrows indicate peaks characteristic of HNT. Diffractograms of cP1.5C before and after heating to 156 °C followed by cooling to RT at 30 °C min^{-1} are compared in the inset. Diffractograms vertically shifted for clarity.

Generally, E′ of each material decreased with increasing temperature, most rapidly in the glass transition region of PLA. At 20 °C, E′ increased with increasing HNT loading to 4.5 GPa for cP6H and cP6H/C20. Obviously, EBS modification of HNT did not increase E′, and the presence of EBS diminished E′ of cP1.5C compared to neat cPLA, similarly to the case of the respective q-materials [28]. This tendency is also visible at 60 and 80 °C. The effect of EBS presence in CP6H/C20 was compensated by better dispersion of HNT.

E′ values of c-materials were higher than those of their q-counterparts reported in Ref. [28], especially at elevated temperature; for example E′ of neat cPLA and cP6H/C20 increased at 20 °C by approx. 8%, and by nearly 40% at 60 °C. It appears that crystallinity and filling can significantly enlarge E′, by approx. 30 and 60% at 20 and 60 °C, respectively, compared to neat qPLA [28].

3.4. Optical properties

Fig. 8 compares the photographs of 0.3 mm thick films positioned on a grid drawn on white paper. The presence of crystallinity, HNT or EBS-modified HNT reduced transparency. The nanofillers caused also yellowing, increasing with their increasing contents. This is corroborated by Fig. 9 showing direct light transmittance (DLT) in λ range from 200 to 1000 nm, comprising UV – Vis – near IR regions. Generally, DLT increased with increasing λ up to 10–50% depending on the material composition and crystallinity. According to ASTM-D1746-03, the transparency of plastic sheets is defined as the transmission of visible light in the short range of 540–560 nm. The DLT values determined at 550 nm for the considered c-materials and the previously studied q-materials (given in brackets) are as follows [28]: cPLA - 8.7% (88%), cP3H - 1.9% (25.6%), cP3H/C10 - 18.6% (29.4%), cP3H/C20 - 17.7% (30%), cP6H - 1.7% (7%), cP6H/C10 - 5.6% (7.5%), cP6H/C20 - 1.9% (3.6%), cP1.5C - 8.0% (25.3%). Interestingly, cPH3/C10 and cPH3/C20 exhibit DLT larger than neat cPLA, possibly due to less scattering on polycrystalline aggregates because of their smaller sizes; the intensity of the scattered light, which escapes detection, depends on the second power of volume of scattering objects. It appears that the transparency can be controlled by suitable filling with HNT and also by the morphology of PLA matrix.

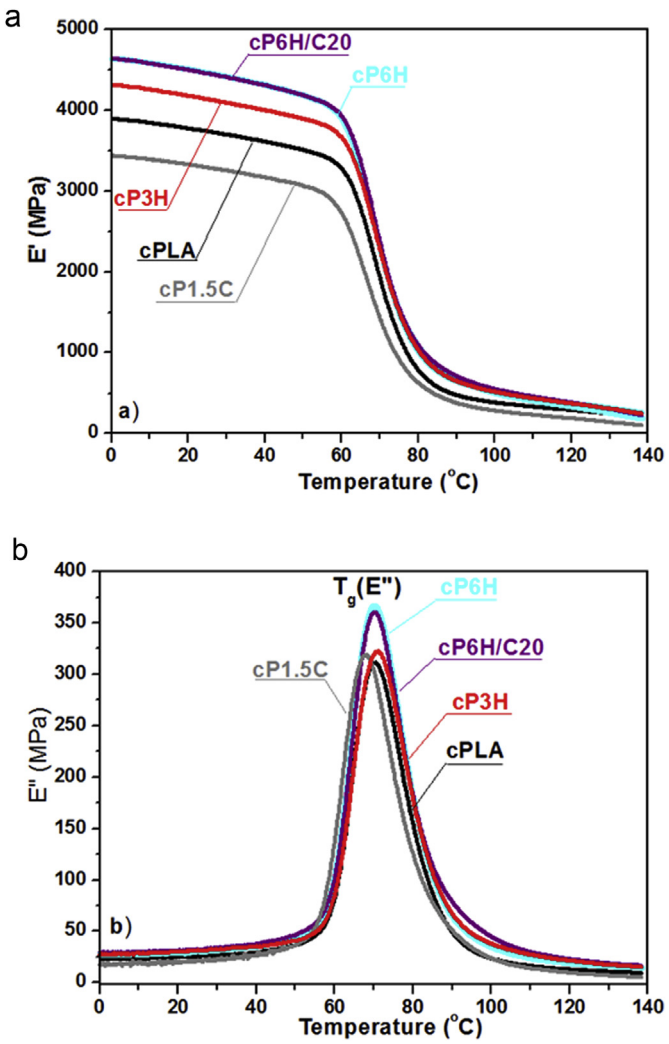

Fig. 7. Temperature dependencies of E' (a) and E" (b) of cPLA, cP1.5C and selected c-nanocomposites.

Table 4
E″ peak temperatures (T_g(E″)), the relative mechanical loss magnitude (MLM) and E′ values determined below and above T_g(E″), at 20, 60 and 80 °C. The numbers in brackets denote the ratios of E′ values to that of neat cPLA.

Sample code	T_g(E″) (°C)	MLM	E' (GPa)		
			20 °C	60 °C	80 °C
cPLA	70.4	1.00	3.8	3.3	0.79
cP3H	71.0	1.12	4.2 (1.11)	3.7 (1.12)	1.0 (1.27)
cP6H	70.1	1.20	4.5 (1.18)	3.9 (1.18)	1.0 (1.27)
cP6H/C20	70.2	1.33	4.5 (1.18)	3.9 (1.18)	1.1 (1.39)
cP1.5C	68.1	1.12	3.3 (0.87)	2.7 (0.82)	0.63 (0.80)

4. Conclusions

Crystalline PLA-based nanocomposites filled with neat HNT and EBS-modified HNT were obtained and analyzed. Amorphous PLA-based films were prepared by compression molding followed by rapid quenching, and then cold-crystallized during heating up to 120 °C and annealing at this temperature. The glass transition temperature of amorphous phase of PLA matrix was not affected by the fillers, although increased because of the presence of crystalline phase. HNT, EBS-treated HNT and EBS nucleated crystallization of PLA matrix and shifted the cold crystallization to lower

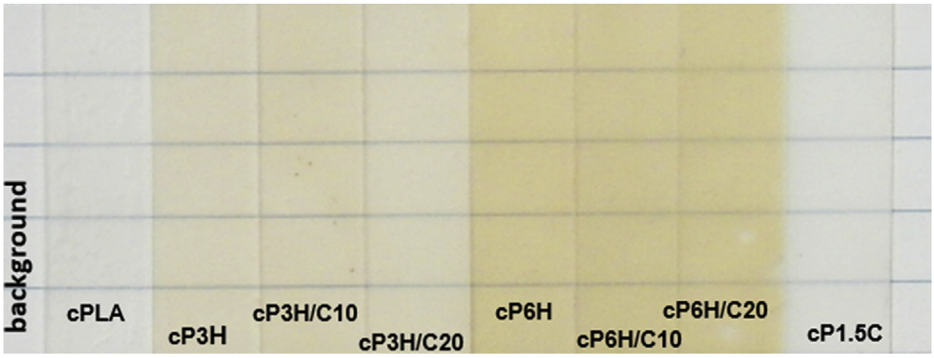

Fig. 8. Illustration of transparency of 0.3 mm thick films placed on a grid drawn on white paper.

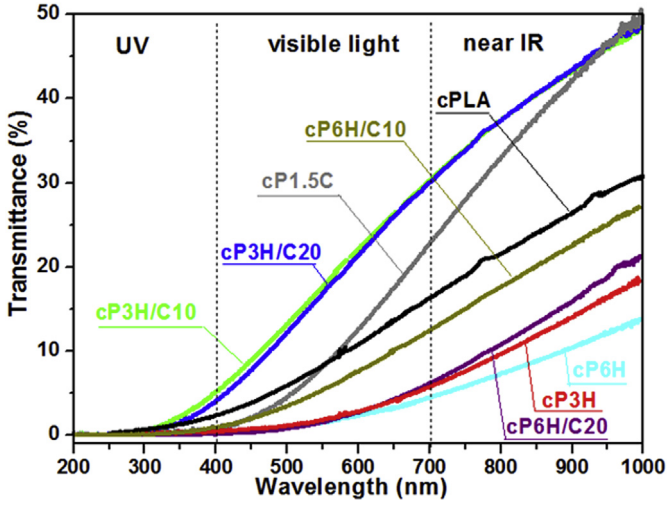

Fig. 9. Comparison of direct light transmittance (DLT) of c-materials.

temperature. Crystallinity degree of PLA matrix in the nanocomposites was similar, however its morphology was strongly affected by the nanofillers. Only in neat crystalline PLA and EBS-free nanocomposites the spherulitic structure was confirmed by the methods used. The storage modulus was enhanced by HNT or EBS-modified HNT as well as by crystallinity of PLA matrix. Owing to the crystallinity and the presence of the nanofillers, the storage modulus at 20 °C and 60 °C increased by up to 30 and 60%, respectively, compared to neat amorphous PLA. Contrary to that, the crystalline PLA blend with EBS exhibited a decreased storage modulus compared to neat crystalline PLA. The direct light transmittance was decreased by HNT and crystallinity but it was also affected by morphology of the PLA matrix; the transmittance of EBS-containing nanocomposites with low HNT loading exceeded that of neat crystalline PLA. The results show that tuning the crystallinity and morphology permits further modification of the properties of the nanocomposites, making them more attractive for engineering applications.

Acknowledgements

The study was conducted Under the Agreement on Scientific Cooperation between the Polish Academy of Sciences and the Fund for Scientific Research – FNRS (FRS -FNRS) Belgium. The statutory fund of the Centre of Molecular and Macromolecular Studies, Polish Academy of Sciences, and the Wallonia Region, Nord-Pas de Calais Region and European Community for the financial support in the frame of the IINTERREG IV - NANOLAC project, are kindly acknowledged. The authors are indebted to Anne–Laure Dechief and Yoann Paint for assistance in the experimental work.

References

[1] K.M. Nampoothiri, N.R. Nair, R.P. John, An overview of the recent developments in polylactide (PLA) research, Biores. Technol. 101 (2010) 8493–8501.
[2] J.R. Dorgan, H.J. Lehermeier, L.I. Palade, J. Cicero, Polylactides: Properties and prospects of an environmentally benign plastic from renewable resorces, Macromol. Symp. 175 (2001) 55–66.
[3] R. Pradhan, M. Misra, L. Erickson, A. Mohanty, Compostability and biodegradation study of PLA–wheat straw and PLA–soy straw based green composites in simulated composting bioreactor, Biores. Technol. 101 (2010) 8489–8491.
[4] G. Kale, R. Auras, S.P. Singh, R. Narayan, Biodegradability of polylactide bottles in real and simulated composting conditions, Polym. Test. 26 (2007) 1049–1061.
[5] M. Kowalczyk, E. Piorkowska, S. Dutkiewicz, P. Sowinski, Toughening of polylactide by blending with a novel aliphatic-aromatic copolyester, Eur. Polym. J. 59 (2014) 59–68.
[6] M. Pluta, E. Piorkowska, Tough and transparent blends of polylactide with block copolymers of ethylene glycol and propylene glycol, Polym. Test. 41 (2015) 209–218.
[7] M. Pluta, E. Piorkowska, Tough crystalline blends of polylactide with block copolymers of ethylene glycol and propylene glycol, Polym. Test. 46 (2015) 79–87.
[8] J.-M. Raquez, Y. Habibi, M. Murariu, P. Dubois, Polylactide (PLA)-based nanocomposites, Prog. Polym. Sci. 38 (2013) 1504–1542.
[9] K. Piekarska, P. Sowinski, E. Piorkowska, Md M. Ul Haque, M. Pracella, Structure and properties of hybrid PLA nanocomposites with inorganic nanofillers and cellulose fibers, Compos. Part A-Appl. Sci. Manuf. 82 (2016) 34–41.
[10] D. Wu, L. Wu, M. Zhang, Y. Zhao, Viscoelasticity and thermal stability of polylactide composites with various functionalized carbon nanotubes, Polym. Degrad. Stab. 93 (2008) 1577–1584.
[11] Y. Wang, Chi-S. Lin, Preparation and characterization of maleated polylactide-functionalized graphite oxide nanocomposites, J. Polym. Res. 21 (2014) article no. 334.
[12] K. Piekarska, E. Piorkowska, J. Bojda, The influence of matrix crystallinity, filler grain size and modification on properties of PLA/calcium carbonate composites, Polym. Test. 62 (2017) 203–209.
[13] M. Murariu, A. Doumbia, L. Bonnaud, A.-L. Dechief, Y. Paint, M. Ferreira, C. Campagne, E. Devaux, P. Dubois, High-performance polylactide/ZnO nanocomposites designed for films and fibers with special end-use properties, Biomacromolecules 12 (2011) 1762–1771.
[14] M.A. Busolo, J.M. Lagaron, Antimicrobial biocomposites of melt-compounded polylactide films containing silver-based engineered clays, J. Plast. Film. Sheet. 29 (2013) 290–305.
[15] A. Zhu, H. Diao, Q. Rong, A. Cai, Preparation and properties of polylactide–silica nanocomposites, J. Appl. Polym. Sci. 116 (2010) 2866–2873.
[16] M. Du, B. Guo, D. Jia, Newly emerging applications of halloysite nanotubes: a review, Polym. Int. 59 (2010) 574–582.
[17] M. Murariu, A.-L. Dechief, Y. Paint, S. Peeterbroeck, L. Bonnaud, P. Dubois, Polylactide (PLA)—halloysite nanocomposites: production, morphology and key-properties, J. Polym. Environ. 20 (2012) 932–943.
[18] G. Gorrasi, R. Pantani, M. Murariu, P. Dubois, PLA/halloysite nanocomposite films: water vapor barrier properties and specific key characteristics, Macromol. Mater. Eng. 299 (2014) 104–115.
[19] Y. Dong, J. Marshall, H.J. Haroosh, S. Mohammadzadehmoghadam, D. Liu, X. Qi, K.-T. Lau, Polylactic acid (PLA)/halloysite nanotube (HNT) composite mats: influence of HNT content and modification, Compos. Part A-Appl. Sci. Manuf. 76 (2015) 28–36.
[20] D. Notta-Cuvier, M. Murariu, J. Odent, R. Delille, A. Bouzouita, J.-M. Raquez,

F. Lauro, P. Dubois, Tailoring polylactide properties for automotive applications: effects of co-addition of halloysite nanotubes and selected plasticizer, Macromol. Mater. Eng. 300 (2015) 684–698.
[21] W.L. Tham, Z.A.M. Ishak, W.S. Chow, Mechanical and thermal properties enhancement of poly(lactic acid)/halloysite nanocomposites by maleic-anhydride functionalized rubber, J. Macromol. Sci. Part B Phys. 53 (2014) 371–382.
[22] W.L. Tham, W.S. Chow, B.T. Poh, Z.A.M. Ishak, Poly(lactic acid)/halloysite nanotube nanocomposites with high impact strength and water barrier properties, J. Comp. Mat. 50 (2016) 3925–3934.
[23] K. Prashantha, B. Lecouvet, M. Sclavons, M.F. Lacrampe, P. Krawczak, Poly(-lactic acid)/halloysite nanotubes nanocomposites: Structure, thermal, and mechanical properties as a function of halloysite treatment, J. Appl. Polym. Sci. 128 (2013) 1895–1903.
[24] W.L. Tham, B.T. Poh, Z.A.M. Ishak, W.S. Chow, Thermal behaviors and mechanical properties of halloysite nanotube-reinforced poly(lactic acid) nanocomposites, J. Therm. Anal. Calorim. 118 (2014) 1639–1647.
[25] M. Murariu, A.-L. Dechief, R. Ramy-Ratiarison, Y. Paint, J.-M. Raquez, P. Dubois, Recent advances in production of poly(lactic acid) (PLA) nanocomposites: a versatile method to tune crystallization properties of PLA, Nanocomposites 1 (2015) 71–82.
[26] A.M. Harris, E.C. Lee, Improving mechanical performance of injection molded PLA by controlling crystallinity, J. Appl. Polym. Sci. 107 (2008) 2246–2255.
[27] Y.-H. Cai, Influence of ethylene bis-stearamide on crystallization behaviour of poly(L-lactide), Asian J. Chem. 25 (2013) 6219–6221.
[28] M. Pluta, J. Bojda, E. Piorkowska, M. Murariu, L. Bonnaud, P. Dubois, The effect of halloysite nanotubes and N,N'- ethylenebis (stearamide) on the properties of polylactide nanocomposites with amorphous matrix, Polym. Test. 61 (2017) 35–45.
[29] S. Saeidlou, M.A. Huneault, H. Li, C.B. Park, Poly(lactic acid) crystallization, Prog. Polym. Sci. 37 (2012) 1657–1677.
[30] M. Pluta, A. Galeski, Crystalline and supermolecular structure of polylactide in relation to the crystallization method, J. Appl. Polym. Sci. 86 (2002) 1386–1395.
[31] J. Bojda, E. Piorkowska, Shear-induced nonisothermal crystallization of two grades of PLA, Polym. Test. 50 (2016) 172–181.
[32] M. Kowalczyk, M. Pluta, E. Piorkowska, N. Krasnikova, Plasticization of polylactide with block copolymers of ethylene glycol and propylene glycol, J. Appl. Polym. Sci. 125 (2012) 4292–4301.
[33] Y. He, T. Wu, J. Wei, Z. Fan, S. Li, Morphological investigation on melt crystallized polylactide homo- and stereocomplex by enzymatic degradation with proteinase K, J. Polym. Sci. Part B Polym. Phys. 46 (2008) 959–970.
[34] M. Rosen, L.C. Franklin, Process for the interconversion of crystalline forms of ethylene bis-stearamide, US Patent 4248792 A, 1981.
[35] E. Zuza, J.M. Ugartemendia, A. Lopez, E. Meaurio, A. Lejardi, J.R. Sarasua, Glass transition behavior and dynamic fragility in polylactides containing mobile and rigid amorphous fractions, Polymer 49 (2008) 4427–4432.
[36] P. Pan, W. Kai, B. Zhu, T. Dong, Y. Inoue, Polymorphous crystallization and multiple melting behavior of poly(L-lactide): Molecular weight dependence, Macromolecules 40 (2007) 6898–6905.
[37] J. Zhang, K. Tashiro, A.J. Domb, H. Tsuji, Confirmation of disorder α form of poly(L-lactic acid) by the X-ray fiber pattern and polarized IR/Raman spectra measured for uniaxially-oriented samples, Macromol. Symp. 242 (2006) 274–278.
[38] M.L. Di Lorenzo, M. Cocca, M. Malinconico, Crystal polymorphism of poly(l-lactic acid) and its influence on thermal properties, Thermochim. Acta 522 (2011) 110–117.
[39] J. Zhang, K. Tashiro, H. Tsuji, A.J. Domb, Disorder-to-order phase transition and multiple melting behavior of poly(L-lactide) investigated by simultaneous measurements of WAXD and DSC, Macromolecules 41 (2008) 1352–1357.
[40] J.R. Sarasua, R.E. Prud'homme, M. Wisniewski, A. Le Borgne, N. Spassky, Crystallization and melting behavior of polylactides, Macromolecules 31 (1998) 3895–3905.
[41] R.S. Stein, M.B. Rhodes, Photographic light scattering by polyethylene films, J. Appl. Phys. 31 (1960) 1873–1884.
[42] Z. Bartczak, A. Galeski, Homogeneous nucleation in polypropylene and its blends by small-angle light scattering, Polymer 31 (1990) 2027–2038.
[43] M. Cocca, M.L. Di Lorenzo, M. Malinconico, V. Frezza, Influence of crystal polymorphism on mechanical and barrier properties of poly(L-lactic acid), Eur. Polym. J. 47 (2011) 1073–1080.
[44] K. Wasanasuk, K. Tashiro, Crystal structure and disorder in Poly(L-lactic acid) δ form (α′ form) and the phase transition mechanism to the ordered α form, Polymer 52 (2011) 6097–6109.
[45] M. Pluta, M. Murariu, M. Alexandre, A. Galeski, P. Dubois, Polylactide compositions. The influence of ageing on the structure, thermal and viscoelastic properties of PLA/calcium sulfate composites, Polym. Degrad. Stab 93 (2008) 925–931.